HHS Public Access

Author manuscript

Mol Microbiol. Author manuscript; available in PMC 2017 October 01.

Published in final edited form as:

Mol Microbiol. 2016 October ; 102(2): 336–348. doi:10.1111/mmi.13463.

Spirochetes flagellar collar protein FlbB has astounding effects in orientation of periplasmic flagella, bacterial shape, motility, and assembly of motors in *Borrelia burgdorferi*

Ki Hwan Moon[a], **Xiaowei Zhao**[b], **Akarsh Manne**[a], **Juyu Wang**[b], **Zhou Yu**[a], **Jun Liu**[b,*], and **Md A. Motaleb**[a,*]

[a]Department of Microbiology and Immunology, Brody School of Medicine, East Carolina University, Greenville, North Carolina, USA

[b]Department of Pathology and Laboratory Medicine, University of Texas Health Science Center, Houston, Texas, USA

SUMMARY

Borrelia burgdorferi, the causative agent of Lyme disease, is a highly motile spirochete, and motility, which is provided by its periplasmic flagella, is critical for every part of the spirochete's enzootic life cycle. Unlike externally flagellated bacteria, spirochetes possess a unique periplasmic flagellar structure called the collar. This spirochete-specific novel component is linked to the flagellar basal body; however, nothing is known about the proteins encoding the collar or their function in any spirochete. To identify a collar protein and determine its function, we employed a comprehensive strategy that included genetic, biochemical, and microscopic analyses. We found that BB0286 (FlbB) is a novel flagellar motor protein, which is located around the flagellar basal body. Deletion of *bb0286* has a profound effect on collar formation, assembly of other flagellar structures, morphology, and motility of the spirochete. Orientation of the flagella toward the cell body is critical for determination of wild-type spirochete's wave-like morphology and motility. Here, we provide the first evidence that FlbB is a key determinant of normal orientation of the flagella and collar assembly.

INTRODUCTION

Lyme disease, which is caused by the spirochete, *Borrelia burgdorferi*, is the most prevalent vector-borne illness in the United States (Mead, 2015). In nature, survival of *B. burgdorferi* depends on migration by the bacteria to sites of colonization in *Ixodes* ticks and mammalian hosts (Zhang *et al.*, 2006; Kuehn, 2013). The spirochete is a motile organism and motility is reported to be crucial for every parts of the spirochete's pathogenic life cycle, e.g., viability of *B. burgdorferi* in ticks, transmission from ticks to mice, persistent infection and dissemination in the mammalian host (Sultan *et al.*, 2013; Sultan *et al.*, 2015; Motaleb *et al.*, 2015).

*Correspondence: MD A. MOTALEB, motalebm@ecu.edu or JUN LIU, Jun.Liu.1@uth.tmc.edu.

The bacterial flagellar motor, such as those examined in *Escherichia coli*, is a highly efficient nano-machine, with a rotation frequency greater than 100 Hz, even though the diameter of the motor is only ca. 45 nm. The flagellum is a complex structure that is composed of three substructures whose assembly requires at least 25 different proteins. The basal body-motor portion of the flagellum is connected to the filament by the rod-hook assembly. When torque is generated by proton (or sodium in some organisms) flux, the flagellum stator rotates the filament propelling the organism to run or swim. The C-ring or switch complex, which is composed of FliG, FliM, and FliN proteins, is attached to the MS-ring basal body (FliF proteins) and stator (MotA-MotB). The C-ring determines whether a motor rotates clock-wise (CW) or counter clock-wise (CCW) (Sowa; Berry, 2008; Chaban *et al.*, 2015; Minamino; Imada, 2015; Kojima, 2015).

Spirochetes are a group of motile bacteria that are distinct from other externally flagellated bacteria such as those seen in *E. coli* in many different aspects (Chen *et al.*, 2011; Charon *et al.*, 2012; Zhao *et al.*, 2014). For example, *B. burgdorferi* is a long organism (10–20 μm) that possesses 7–11 flagella inserted at each pole of the cell (up to 22 flagella per cell). Unlike *E. coli*, *B. burgdorferi* flagella are located between the outer membrane and peptidoglycan layer i.e., in the periplasmic space (Kudryashev *et al.*, 2009; Charon *et al.*, 2009; Charon *et al.*, 2012; Wolgemuth, 2015; Motaleb *et al.*, 2015). *B. burgdorferi* motility and chemotaxis genes are controlled by housekeeping σ^{70} promoters. This results in the flagella of this spirochete being assembled in a sequential manner. Moreover, the flagellar motors of spirochetes, specifically those of *B. burgdorferi*, are much larger than *E. coli* motors (~80 *vs.* ~45 nm) and thus require more gene products for their assembly (Chevance; Hughes, 2008; Charon *et al.*, 2012; Zhao *et al.*, 2013).

The periplasmic flagella originate near the cell poles and extend toward the other pole of the cell or toward the cell body. In motile cells, the periplasmic flagellar filaments form a ribbon-like structure that wraps around the cell body, resulting in a distinctive flat-wave morphology (Kudryashev *et al.*, 2009; Charon *et al.*, 2009; Sultan *et al.*, 2015; Motaleb *et al.*, 2015). It has been proposed that the spirochete's flagella rotate asymmetrically during a "run" mode, i.e., flagella at one pole rotate CW whereas the flagella at the other end rotate CCW. When flagella at both poles rotate in the same direction, the spirochete flexes/tumbles (Li *et al.*, 2002; Charon *et al.*, 2012). While flagella in most other bacteria are involved in motility, periplasmic flagella in *B. burgdorferi* determine the cellular morphology as well as motility. For example, a mutant that lacks FlaB encoding the protein component of the periplasmic flagellar filaments produces a rod-shaped cell in addition to being non-motile (Motaleb *et al.*, 2000; Sultan *et al.*, 2013). Due to their involvement in cellular morphology and the fact that these flagella rotate within the periplasmic space, it is not surprising that spirochetes possess extra or unique flagellar structures that offer flexibility or rigidity that is required to rotate their flagella within the periplasmic space. Recently, cryo-electron tomography (cryo-ET) of spirochete flagellar motors revealed unique features that are absent from all other bacterial motors studied to-date. One of these structures is called the "collar" (Murphy *et al.*, 2006; Liu *et al.*, 2010; Chen *et al.*, 2011; Raddi *et al.*, 2012; Zhao *et al.*, 2014). The collar is appeared to locate adjacent to FliL. FliL homologs are found in several species of bacteria and its function is distinct in those organisms (Jenal *et al.*, 1994; Belas; Suvanasuthi, 2005; Attmannspacher *et al.*, 2008; Suaste-Olmos *et al.*, 2010; Kudryashev *et*

al., 2010; Motaleb *et al.*, 2011; Zhu *et al.*, 2015). In *B. burgdorferi*, we found that periplasmic flagellar filaments were partially and abnormally tilted toward the cell pole in the Δ*fliL* mutant (Motaleb *et al.*, 2011).

Importantly, the collar is apparently integrated with the major components of the periplasmic flagella such as the MS-ring. Because of these connections and its central location in the motor, we hypothesize that the collar is critical for flagellar assembly as well as for providing proper rigidity or flexibility of flagella during rotation. However, nothing is known about the proteins encoding the unique collar structure or their function in any spirochete. In this communication, we show that mutations in *bb0286 (flbB*) has a profound effect on collar formation, flagellar orientation, morphology, motility, and the assembly of FliL as well as the stator. Moreover, using green fluorescent protein (GFP) we determined the location of FlbB in the collar. A mechanism underlying the orientation of the periplasmic flagella is also demonstrated.

RESULTS

Identification of a protein encoding the collar structure

Genomic analysis suggests that over 50 genes or 5–6% of the *B. burgdorferi* genome are potentially involved in motility and chemotaxis (Fraser *et al.*, 1997; Charon *et al.*, 2012). In order to identify proteins involved in the collar structure, we employed a strategy by subtracting common gene homologs that are present in other bacterial genomes especially those with externally flagellated bacteria whose motors have been determined by cryo-ET (Chen *et al.*, 2011). To ensure that we did not overlook any gene that may share low homology but could encode a collar protein, we systematically mutated almost all genes annotated as “flagellar/motility-related” in the *B. burgdorferi* genome (Fraser *et al.*, 1997; Charon *et al.*, 2012) (our unpublished observation). Through these analyses, BB0286 (FlbB) was identified as a potential candidate for the collar structure. *flbB* is a spirochete-specific gene that is located within the flagellar *flgB* polycistronic operon, increasing the likelihood that this protein may encode for a flagellar gene (Ge *et al.*, 1997; Ge and Charon, 1997; Charon *et al.*, 2012). FlbB is a small protein (205 a.a.) that possess a transmembrane domain at its N-terminal end and shares no significant amino acid sequence identity with proteins from non-spirochetal bacteria (data not shown; see below).

Δ*flbB* mutant cells are rod-shaped and non-motile

We deleted the *flbB* gene by using a promoter-less kanamycin resistance cassette that results in nonpolar mutations (Fig. 1A) (Sultan *et al.*, 2010; Pitzer *et al.*, 2011; Sultan *et al.*, 2011). PCR analysis of the kanamycin-resistant *B. burgdorferi* clones confirmed the deletion of the *flbB* (data not shown). Immunoblotting with anti-FlbB antisera indicated that FlbB protein synthesis was inhibited in the Δ*flbB* mutant cells; yet, expression of proteins encoded by genes downstream of *flbB*, i.e., *flgE*, *motB*, and *fliL*, were not altered in the mutant cells compared to the wild-type *B. burgdorferi* (Fig. 1B). This suggests that the mutant phenotype is due solely to loss of *flbB* function (see below). Although the mutant did not exhibit a polar effect on downstream genes expression, we attempted to complement the Δ*flbB* mutant both *in cis* (genetic recombination) and *in trans* (using a shuttle vector). While multiple

attempts to genetically complement the Δ*flbB* mutant have failed, we report our findings with the mutant as others have done in the past (Stewart *et al.*, 2008; Rogers *et al.*, 2009; Dresser *et al.*, 2009; Hyde *et al.*, 2009; Pappas *et al.*, 2011; Motaleb *et al.*, 2011; Brisson *et al.*, 2012; Miller *et al.*, 2013).

Dark-field microscopy and swarm plate assays were used to assess cell morphology and motility of Δ*flbB* cells (Motaleb *et al.*, 2007; Moon *et al.*, 2016). These measurements indicated that the mutant cells are non-motile and display a rod-shaped morphology (Fig. 2), despite the synthesis of periplasmic flagella, FlaB, albeit at a reduced level compared to the wild-type (Fig. 1B). Furthermore, swarm plate motility assays indicate that the mutant cells produced colony diameters that are significantly smaller than the wild-type cells (~1 mm *vs.* ~6 mm swarm produced by the wild-type; Fig. S1). The morphology and motility phenotypes of the Δ*flbB* mutant cells are similar to the non-motile, rod-shaped Δ*flaB* mutants that lack flagellar filaments (Motaleb *et al.*, 2000; Sultan *et al.*, 2013). Taken together, our results indicate that FlbB is important for morphology and motility of *B. burgdorferi*.

Δ*flbB* mutant displays abnormal periplasmic flagellar orientation

Previous studies showed that periplasmic flagella are crucial not only for motility but also for the cellular flat-wave morphology of *B. burgdorferi* (Motaleb *et al.*, 2000; Sultan *et al.*, 2013). Because the Δ*flbB* mutant cells synthesize periplasmic flagella but are rod-shaped, we investigated the basis of those defects using cryo-ET (Fig. 3). Our reconstructions of the native cellular structures shown in Figs. 3C, D indicate that the wild-type periplasmic flagella form ribbon-like structures that are oriented inwards toward the center of the cell. In contrast, the mutant's periplasmic flagella are short and the flagellar ribbon is distorted. Most striking and opposite to wild-type, Δ*flbB* flagella are oriented abnormally toward the cell pole (compare Fig. 3A–B with 3C–D or Movie 1 with Movie 2). In fact, the majority of periplasmic flagella (82% *vs.* 1–2% in the wild-type) are found to be abnormally oriented toward the cell pole in the mutant cells (Table 1; Movies 1–2). These results indicate that FlbB is essential for normal orientation of periplasmic flagella (toward the cell body).

The collar structure is absent in the Δ*flbB* mutant cells

We compared the motor structures in wild-type and the Δ*flbB* mutant cells by cryo-ET and found that the collar structure is absent from the mutant's periplasmic flagella (Figs. 4A, B). To reveal the motor structure in detail, we used subtomogram averaging to analyze approximately 1000 motor structures extracted from tomographic reconstructions. The averaged structure reveals major features of the flagellar motor, such as the export apparatus, the C-ring, the MS-ring, the rod, and the P-ring (Fig. 4C). These major features of the wild-type motor are also detected in the Δ*flbB* motor (Fig. 4D). However, a large portion of densities surrounding the central rod and the P-ring are absent in the Δ*flbB* motor (Fig. 4D). Specifically, the Δ*flbB* motor lacks the collar structure detected in wild-type cells (compare Figs. 4C, E with 4D, F).

By comparing structures from a deletion mutation in *motB* (J. Liu and M. Motaleb-unpublished), *fliL* (Motaleb *et al.*, 2011), and the current Δ*flbB* strain, we were able to

define the 3D structure of the collar and the stator (Figs. 4E, G). The overall dimension of the collar is ~71 nm in diameter and ~24 nm in height. This unique structure consists of two major layers along the radial direction—for clarity, labeled here as the inner core domain and the outer turbine-like domain (Fig. 4G). The inner domain of the intact collar appears to consist of 16 truss-like subassemblies joined together to form a chamber-like structure that surrounds the rod and the P-ring (Figs. 4E, G). FliL is attached to each subassembly at the membrane region (Figs. 4C, G). The outer domain—the sixteen extended "turbine blades"—is the most distinct feature appearing in the spirochetal flagellar motor. Sixteen stator units are inserted between two adjacent "turbine blades", forming a stator ring that packs around the C-ring in the cytoplasm (Figs. 4E, G). Furthermore, the stator (MotA-MotB) and FliL structures are also disappeared in the mutant even though MotB and FliL proteins are stably expressed at wild-type levels, suggesting that FlbB/collar is important for the assembly of those flagellar structures (compare Figs. 4C, E with 4D, F). Together, our cryo-ET data indicate that FlbB is essential for the formation of the collar structure and the assembly or stability of FliL and the stator.

FlbB—FliL interactions

As shown above, majority of Δ*flbB* mutant's periplasmic flagella are abnormally tilted toward the cell pole. Interestingly, we observed a similar phenotype with our Δ*fliL* mutant cells (Table 1) (Motaleb *et al.*, 2011). These results led us to predict that (a) FlbB and FliL proteins interact and direct the periplasmic flagella to orient toward the cell body but not the cell pole; (b) FlbB and FliL are located in close proximity to each other; and (c) FlbB/collar is assembled before FliL and the stator because the FliL and stator structures are not assembled in the Δ*flbB*. To determine if FlbB interacts with FliL, we performed co-immunoprecipitation (co-IP) assays with wild-type and Δ*flbB* cell extracts. Our co-IP data indicate that FlbB specifically interacts with FliL (Fig. 5). The FlbB-FliL binding is verified further by using an alternative bacterial two-hybrid assay (BACTH). Our two-hybrid assays also confirmed that FlbB interacts with FliL (Fig. S2). These FliL-FlbB interaction results suggest that FlbB is located adjacent to the FliL, near the base of the collar structure (see below).

Our motor structures show that the periplasmic domain of the stator is adjacent to the collar and that the stator structure is missing in the Δ*flbB* (Fig. 4). To test if there is any interaction between the stator and FlbB, and this interaction is important for the assembly of the stator, we performed co-IP and BACTH assays, as described above. Using these assays, we failed to detect any FlbB-MotA or FlbB-MotB interaction (data not shown), indicating that FlbB is not directly interacting with the stator and supporting our proposal that FlbB is just a small part of the collar that is located at its base (below).

Localization of FlbB by GFP fusion

To determine the location of FlbB in the periplasmic flagella, the gene encoding GFP was fused at the 3′-end of *flbB* (*flbB-gfp*) and then ligated such that *flgB* promoter drives the expression of *flbB-gfp* (P_{flgB}-*flbB-gfp*) from the shuttle vector pBSV2G. The placement of *gfp* at the 3′-end of *flbB* is suitable for the expression of FlbB-GFP since the N-terminal region (7–29 amino acid residues) of FlbB is found to possess a transmembrane domain

using TMHMM Server, ver. 2.0 (Fig. S3) (Sonnhammer *et al.*, 1998; Krogh *et al.*, 2001). Subsequent introduction of pBSV2G::P_{flgB}-*flbB-gfp* into Δ*flbB* mutant cells resulted in expression of FlbB-GFP, as confirmed by immunoblotting using anti-GFP and anti-FlbB (not shown). Confocal microscopy shows the FlbB-GFP clusters at ~73% of the cell tips of the Δ*flbB*/pBSV2G::P_{flgB}-*flbB-gfp* cells where motors are typically located (Δ*flbB/flbB-GFP* cells; Fig. 6, right). As expected, this pattern (FlbB-GFP clusters) was not observed in the wild-type cells expressing only GFP using pBSV2G::P_{flgB}-*gfp* plasmid (wild-type GFP; Fig. 6, left) or in the Δ*flbB* mutant negative control cells that does not express GFP (not shown).

To conclusively determine FlbB location, cryo-ET and subtomogram averaging were utilized to visualize the motor structure of the Δ*flbB/flbB-GFP* cells. Compared to the cellular density of Δ*flbB* motor, the Δ*flbB/flbB-GFP* motor shows extra densities near the basal body MS-ring structure as shown in Fig. 7, suggesting the location of FlbB-GFP. Together, these data imply that FlbB proteins are located at the base of the collar and they are anchored to the cytoplasmic membrane to form the base for the assembly of the collar complex.

DISCUSSION

Despite the fact that periplasmic flagellar motility is crucial for host colonization or disease production by the spirochetes including *B. burgdorferi*, there is still very limited knowledge about what genes encode for the spirochete-specific flagellar components. FlbB identified as a collar protein in this communication has profound effects in motility, morphology, orientation of periplasmic flagella, and assembly of motor proteins. The Δ*flbB* mutant cells are rod-shaped and non-motile despite the possession of periplasmic flagella (Figs. 1, 2, and 3), however, those flagella are inactive due to their missing stators (Figs. 4D, F). Stator proteins use proton flux to produce torque in order for the flagella to rotate, which in turn enables the organism to translocate. Because the periplasmic flagella are oriented abnormally and their stators are missing, it was obvious that those *B. burgdorferi* mutant cells exhibited rod-shaped and non-motile phenotypes. However, the number of periplasmic flagella or level of flagellar filament FlaB protein is reduced in the mutant compared to the wild-type cells (Fig. 1B). The *flaB* gene is not genetically linked with the targeted *flbB* or other genes in the *flgB* operon. However, we observed this reduced FlaB protein synthesis or fewer flagellar filaments not only in Δ*flbB* but also in other non-motile mutants such as Δ*motB* (Sultan *et al.*, 2015). These observations suggest that the stator or collar-stator is important for the wild-type level of periplasmic flagellar filament synthesis in *B. burgdorferi*.

One of the most remarkable findings here is the abnormal orientation of flagella in the Δ*flbB* mutant (Fig. 3; Table 1; Movie 2). Normal orientation of the flagella toward the cell body and not the cell pole is critical in producing the wild-type spirochete's wave-like morphology and smooth swimming (Figs. 2 and 3) (Motaleb *et al.*, 2011). We have previously reported that FliL is partially responsible for determination of flagellar orientation (Motaleb *et al.*, 2011). As shown in Fig. 3 and Table 1, 82% of the flagella in the Δ*flbB* are abnormally oriented. Thus, based on Δ*flbB* and Δ*fliL* flagellar orientation phenotypes as well as protein-protein interaction data shown in Figs. 5 and S2, we propose

that FlbB/collar—FliL structures enforce the periplasmic flagella to orient toward the cell body—an observation that has never been demonstrated in any spirochete. We, however, postulate that this irregular periplasmic flagellar phenotype associated with the mutant is a combined effect of collar-stator-FliL rather than just the FlbB/collar since the stator and FliL structures were diminished along with the collar (in the Δ*flbB* mutant). Moreover, it is important to note that the Δ*flbB* mutant was not complemented. Thus, the phenotypes observed with the mutant could be due to a secondary mutation elsewhere in the genome rather than just because of the deletion of *flbB* even though the mutant is non-polar (Fig. 1B).

The stator and FliL structures were disappeared in the mutants despite the synthesis of MotB and FliL proteins at the wild-type levels (Figs. 1 and 4D, F), indicating that those structures were not assembled due to the lack of the collar structure. It is noteworthy to mention that the collar structure is intact in our Δ*motB* (J. Liu and M. Motaleb-unpublished) or Δ*fliL* mutants (Motaleb *et al.*, 2011). Furthermore, the stator is intact in the Δ*fliL* mutant—a very good indication that FliL and stator structures were diminished not because of a secondary alteration or polar effect (Motaleb *et al.*, 2011). These results also suggest that the collar is assembled before FliL or the stator. Moreover, FliL and stator structures were not assembled in the Δ*flbB* likely because the collar provides the stability/foundation for those two motor structures similar to what was observed with the flagellar filament proteins, FlaA and FlaB. FlaA and FlaB proteins interact and we found that unless the filament FlaB is synthesized and assembled, FlaA protein is not assembled in the Δ*flaB* (Motaleb *et al.*, 2000; Sultan *et al.*, 2013).

In *E. coli* or *Salmonella typhimurium*, FliL was reported to interact with the stator (Partridge *et al.*, 2015). However, we could not detect any interactions between FliL-MotA, FliL-MotB, FlbB-MotA, or FlbB-MotB. These results suggest that FliL or FlbB may not interact with the stator directly. Alternatively, our BACTH vectors (pKT25 and pUT18C) could not express MotA or MotB properly or our co-IP reaction conditions were not optimized. However, in *Rhodobacter sphaeroides*, FliL is able to interact with itself but not with the MotB leading to the proposal that FliL may participate in coupling with the flagellar stator in an indirect manner (Suaste-Olmos *et al.*, 2010). Moreover, in *Vibrio alginolyticus*, FliL was suggested to interact with the stator directly or indirectly (Zhu *et al.*, 2015). Subsequently, we propose that *B. burgdorferi* FliL (or FlbB/collar) interacts with the stator indirectly using a yet to be identified protein(s) which is important for the assembly of the stator.

It is noteworthy that the full collar structure was not assembled in the Δ*flbB* cells expressing FlbB-GFP (Fig. 7), and morphology and motility phenotype were also not restored in those cells (not shown). This result is not surprising because in order for the collar structure or function to be restored in the Δ*flbB*, the FlbB-GFP protein's stoichiometry should be the same as that of other collar proteins since most motor complexes maintain a ratio (such as the FliG:FliM:FliN protein copies in a switch complex are 34:34:100, and MotA:MotB ratio is 4:2 in a stator complex) (Blair, 2003; Kojima; Blair, 2004; Leake *et al.*, 2006). When GFP or mCherry was fused with flagellar motor MotA or MotB or their homologs, assembly

and/or function was reported to be abolished in other bacteria (Fukuoka *et al.*, 2009; Paulick *et al.*, 2009).

The collar is a colossal structural component of the periplasmic flagella. It is noticeably larger than the C-ring or stator (Fig. 4). Considering that the C-ring is composed of three proteins (FliG, FliM, and FliN), the collar is likely comprised of multiple proteins. FlbB is a small protein (205 amino acids) that is comparable to its binding partner FliL (178 amino acids) or MotB (260 amino acids). FliL appears to form a small and elongated structure right next to the edge of the collar (Figs. 4C, G) (Motaleb *et al.*, 2011). Therefore, we propose that FlbB is arranged in a small structure at the base of the collar by embedding in the cytoplasmic membrane using its transmembrane domain (Figs. 7 and S3). Other (unidentified) collar proteins are expected to assemble onto the FlbB base. As such, deletion of *flbB* had a dramatic effect on the entire collar, and thus, its associated structures are not assembled in the Δ*flbB*.

Altogether, our data demonstrate that the collar is a highly complex structure that has profound impacts in *B. burgdorferi*. Importantly, we show for the first time that FlbB assembles around the flagellar basal body and plays critical roles in collar formation. Furthermore, we provided the first 3D structure of the collar and revealed its unprecedented complexity. Moreover, we show that FlbB and FliL are crucial for normal orientation of periplasmic flagella.

EXPERIMENTAL PROCEDURES

Bacterial strains and growth conditions

High-passage, avirulent *B. burgdorferi* strain B31-A was used as a wild-type clone throughout the study (Bono *et al.*, 2000; Elias *et al.*, 2002). Construction of a *flbB* (*bb0286*) deletion mutation was achieved as described below. *B. burgdorferi* cells were cultured in liquid Barbour-Stoenner-Kelly (BSK-II) medium, and plating BSK was prepared using 0.4% agarose (Motaleb *et al.*, 2007; Sultan *et al.*, 2013). Cells were grown at 35°C in a 2.5% CO_2 incubator as described previously (Motaleb *et al.*, 2007). *E. coli* cells were grown at 30°C or 37°C in Luria-Bertani (LB) broth or LB agar (Bertani, 1951). Antibiotics, indicators, and inducers, when required, were included in the bacterial culture medium with the following concentrations: 100 μg ml^{-1} ampicillin, 50 μg ml^{-1} kanamycin, 100 μg ml^{-1} spectinomycin, 40 μg ml^{-1} gentamicin, 80 μg ml^{-1} 5-bromo-4-chloro-3-indolyl-β-D-galactopyranoside (X-gal), 0.5 mM isopropyl-β-D-thiogalactoside (IPTG).

Construction of the flbB-deletion mutant

Construction of the *flbB*-deletion plasmids, electroporation, and plating conditions were described previously (Motaleb *et al.*, 2007; Sultan *et al.*, 2010; Pitzer *et al.*, 2011; Sultan *et al.*, 2013). Briefly, the 5′-(1198 bp), and 3′-flaking (432 bp) DNA of *flbB* gene were amplified by PCR from chromosomal DNA of *B. burgdorferi* strain B31-A using primers FlbB.KO.P1F (GACGATTAGAACCTACTTTCG) and FlbB.KO.P1R (TAAAATTGCTTTTAACTATTATTCACTTTCATTCC), and FlbB.KO.P2F (CGATGAGTTTTTCTAATCATTGGAGTAGTGTG) and FlbB.KO.P2R

(TTGGTCCTTAGAGTCATCT), respectively. Promoter-less kanamycin resistance cassette [*Pl-kan*, 846 bp] was similarly PCR amplified from P_{flgB}-*aph1* using primers FlbB.KO.KanF (GGAATGAAAGTGAATAATAGTTAAAAGCAATTTTA) and FlbB.KO.KanR (CACACTACTCCAATGATTAGAAAAACTCATCG) (Sultan *et al.*, 2010). These three pieces of DNA fragments were linked by overlapping PCR, yielding *bb0285-Pl-kan-bb0287* (*flbB*_KO_*Pl-kan*), then cloned into the pGEM-T Easy (Promega Inc.), yielding plasmid Teasy::*flbB*_KO_*Pl-kan*. Competent B31-A cells were electroporated with *flbB*_KO_*Pl-kan* PCR amplified linear DNA. The transformants were selected with 200 μg ml^{-1} kanamycin. The kanamycin-resistant transformants were isolated and confirmed the replacement of *flbB* gene with the *Pl-kan* by PCR, and lack of FlbB protein expression was confirmed by immunoblotting as described below.

Construction of a plasmid expressing FlbB-GFP

To construct a *B. burgdorferi* strain that expresses GFP coupled with FlbB, the *flgB* promoter (P_{flgB}), and *flbB* gene were PCR amplified from chromosomal DNA of strain B31-A using primers P_{flgB}-*Bam*HI.F (GGATCCCGAGCTTCAAGGAAGATTTCC) and P_{flgB}-*flbB*.R (ATAAAAAATTATTCACATGGAAACCTCCCTCATTTAAAA), and P_{flgB}-*flbB*.F (TGAGGGAGGTTTCCATGTGAATAATTTTTTATCGTTC) and *flbB-gfp*.R (TCTTCTCCTTTACTCTCCAATGAACTAACAG), respectively (*Bam*HI restriction site is underlined). *gfp* was PCR amplified from pMC2498 plasmid using primers *flbB-gfp*.R (CTGTTAGTTCATTGGAGAGTAAAGGAGAAGA) and *gfp-Hin*dIII.R (AAGCTTCTATTTGTATAGTTCATCCATGCCATG) (*Hin*dIII restriction site is underlined) (Caimano *et al.*, 2015; Iyer *et al.*, 2015). These three pieces of DNA fragments were linked by overlapping PCR and cloned into the pGEM-T Easy, yielding plasmid Teasy::P_{flgB}-*flbB-gfp*. This and the *B. burgdorferi* shuttle vector pBSV2G were digested with *Bam*HI and *Hin*dIII, and ligated to yield pBSV2G::P_{flgB}-*flbB-gfp* (Elias *et al.*, 2003). Approximately 50 μg of pBSV2G::P_{flgB}-*flbB-gfp* plasmid DNA was electroporated into the Δ*flbB* mutant cells. Transformants were selected with kanamycin and gentamicin. Resistant transformants were analyzed by PCR to confirm the presence of the pBSV2G::P_{flgB}-*flbB-gfp* plasmids in the transformants (Δ*flbB/flbB-GFP* cells). Furthermore, the expression of GFP and FlbB proteins in the Δ*flbB/flbB-GFP* cells were confirmed by immunoblotting with *B. burgdorferi* FlbB-specific polyclonal and Anti-GFP monoclonal (Roche Life Science) antibodies, respectively. Anti-FlbB was raised in rabbits which immunized with purified recombinant His_6-FlbB, as described (Alpha Diagnostic International) (Motaleb *et al.*, 2011).

SDS-PAGE and immunoblot analyses

Sodium dodecyl sulfate-polyacrylamide gel electrophoresis (SDS-PAGE) and immunoblotting with an enhanced chemiluminescent detection method (GE Health Inc.) were carried out as reported previously (Motaleb *et al.*, 2000; Sultan *et al.*, 2013). The concentration of protein in cell lysates was determined by a Bio-Rad protein assay kit. Unless otherwise noted, 10 μg of lysate protein was subjected to SDS-PAGE and immunoblotting using proper antibodies.

Dark-field microscopy and measurement of colony size

Growing *B. burgdorferi* cells (2–4 $\times 10^7$ cells ml^{-1}) were imaged using a Zeiss Imager M1 dark-field microscope connected to a Zeiss AxioCam MRc digital camera to determine morphology. For measurement of *B. burgdorferi* colony swarm diameter, approximately 20 to 50 cells were plated on semi-solid BSK-II medium containing 0.4% agarose. Four weeks after inoculation, we measured the diameter of 20 representative colonies from each clone (Moon *et al.*, 2016).

Confocal laser scanning microscopy

B. burgdorferi cells were examined with a confocal microscope (LSM 510; Carl Zeiss, Inc., Thornwood, NY, USA) using 488 nm Argon ion laser excitation and a 505–550 bandpass filter to collect GFP fluorescence emission, with simultaneous collection of a transmitted light image using differential interference contrast (DIC) optics. Images were acquired and analyzed using Zen 2009 software (Zeiss Inc.).

Cryo-electron tomography (cryo-ET) and subtomogram averaging

Frozen-hydrated specimens were prepared as described previously (Zhao *et al.*, 2013; Sultan *et al.*, 2015). Briefly, growing *B. burgdorferi* wild-type, Δ*flbB* mutant, and *flbB-GFP* cells were harvested at low 1,500×g speed, and suspended in 40 μl phosphate buffered saline (PBS, pH 7.4) at a final concentration of ~2×10^9 cells ml^{-1}. Resuspended cells were mixed with 10 nm gold clusters, then 5 μl was deposited onto freshly glow-discharged holey carbon grids for 1 min. Grids were blotted with filter paper to remove excess fluid, followed by rapid freezing in liquid ethane maintained at −180°C using a gravity-driven plunger apparatus (Liu *et al.*, 2009; Zhao *et al.*, 2013). The resulting frozen-hydrated specimens were imaged at −170°C using a Polara G2 electron microscope (FEI Company) equipped with a field emission gun and a K2 direct electron detector (Gatan). The microscope was operated at 300 kV with a magnification of ×9,400, resulting in an effective pixel size of 4.6 Å. Using the FEI batch tomography program, low-dose single-axis tilt series were collected from each bacterium at a −6 μm defocus with a cumulative dose of ~60 $e^-/Å^2$ distributed over 60 images. Tilt angles were in the range of −60° and +60° with an angular increment of 2°. Tilt series were aligned and reconstructed using IMOD software and tomoauto (Kremer *et al.*, 1996; Hu *et al.*, 2015).

In total, 285 and 190 reconstructions were generated from Δ*flbB* mutant and *flbB-GFP* cells, respectively. A total of 1,742 motor sub-tomograms (256×256×256 voxels) were visually identified, then extracted from the reconstructions. The initial orientation of each particle was estimated by the C-ring and the hook, thereby providing two of the three Euler angles. To accelerate image analysis, 4×4×4 binned sub-tomograms (64×64×64 voxels) were used for initial alignment. The original data was then used for the refinement and averaging as described previously (Liu *et al.*, 2009; Zhao *et al.*, 2013).

3D visualization

Reconstructions of *B. burgdorferi* cells were visualized and segmented manually using IMOD (Kremer *et al.*, 1996). UCSF Chimera, a visualization system for exploratory research

and analysis, was utilized for 3-D surface rendering of sub-tomogram averages (Pettersen *et al.*, 2004).

Co-immunoprecipitation (co-IP)

FlbB and FliL protein-protein interactions were determined using a Dynabeads® Protein A Immunoprecipitation kit, according to the manufacture's protocol (Novex Inc.). Briefly, 36 μg of rabbit polyclonal FlbB antibodies were diluted in 600 μl of PBS with 0.01% Tween 20, and then coupled the antibody with 1.5 mg of Dynabeads. To prepare cell extracts, wild-type or Δ*flbB* mutant *B. burgdorferi* cells were harvested. Cell pellets were resuspended in PBS with 0.01% Tween 20 and then lysed by sonication. Sonicated cell extracts were centrifuged at 16,000 × g for 15 min at 4°C to remove bacterial debris. Approximately 750 μg cell extracts were incubated with FlbB antibody-conjugated Dynabeads with gentle shaking for 10 min at room temperature, and washed with 1 ml of washing buffer for four times. 50 μl of SDS loading dye was added directly to the FlbB antibody-conjugated Dynabeads after the washes, and then heated for 10 minutes in boiling water bath. The boiled samples were subjected to SDS-PAGE and immunoblotting using *B. burgdorferi* FliL-specific antibodies (Motaleb *et al.*, 2011). FlbB-MotB and FliL-MotB co-IP assays were similarly performed using *B. burgdorferi* FlbB, FliL, or MotB-specific polyclonal antisera (Sultan *et al.*, 2015).

Bacterial two-hybrid system

Protein-protein interactions between FlbB and FliL were measured with the bacterial adenylate cyclase two hybrid system, according to the manufacture's protocol (BACTH; Euromedex Inc.). Briefly, *flbB* and *fliL* genes were amplified by PCR from chromosomal DNA of *B. burgdorferi* strain B31-A using primers FlbB.*Bam*HI.F (**GGATCC**CAATAATTTTTTATCG) and FlbB.*Kpn*I.R (**GGTACCCTC**CAATGAACTAAC), and FliL.*Bam*HI.F (**GGATCC**CCCTAATAAAGACG) and FliL.*Kpn*I.R (**GGTACC**CATATCAAAAATATCAATT), respectively (restriction enzyme sites are shown in bold). These DNA fragments were cloned into the pUT18C and pKT25. Both pUT18C::*flbB* (or *fliL*) and pKT25::*fliL* (or *flbB*) were co-transformed into the BTH101 *E. coli* host cell. Transformants were grown on LB plates containing X-gal, ampicillin, and kanamycin. Appearance of blue colored colonies in those plates is an indication of a positive protein-protein interaction. FliL-MotA, FliL-MotB, FlbB-MotA, and FlbB-MotB interactions were performed as described for FliL-FlbB.

Statistical analysis

A paired Student's *t*-test was used to determine statistical significance. A *P*-value of ≤0.05 between samples was considered significant.

Supplementary Material

Refer to Web version on PubMed Central for supplementary material.

Acknowledgments

We thank Dr. Robert Belas for critical reading of this manuscript and Dr. Douglas Weidner for help in confocal microscopy. This work was supported by grants from National Institute of Allergy and Infectious Diseases (NIAID) (R01AI087946, R21AI113014), National Institute of Arthritis and Musculoskeletal and Skin Diseases (NIAMS) (R01AR060834), and Welch Foundation (AU-1714).

References

Attmannspacher U, Scharf BE, Harshey RM. FliL is essential for swarming: motor rotation in absence of FliL fractures the flagellar rod in swarmer cells of *Salmonella enterica*. Mol Microbiol. 2008; 68:328–341. [PubMed: 18284590]

Belas R, Suvanasuthi R. The ability of *Proteus mirabilis* to sense surfaces and regulate virulence gene expression involves FliL, a flagellar basal body protein. J Bacteriol. 2005; 187:6789–6803. [PubMed: 16166542]

Bertani G. Studies on lysogenesis. I. The mode of phage liberation by lysogenic *Escherichia coli*. J Bacteriol. 1951; 62:293–300. [PubMed: 14888646]

Blair DF. Flagellar movement driven by proton translocation. FEBS Lett. 2003; 545:86–95. [PubMed: 12788496]

Bono JL, Elias AF, Kupko JJ 3rd, Stevenson B, Tilly K, Rosa P. Efficient targeted mutagenesis in *Borrelia burgdorferi*. J Bacteriol. 2000; 182:2445–2452. [PubMed: 10762244]

Brisson D, Drecktrah D, Eggers CH, Samuels DS. Genetics of *Borrelia burgdorferi*. Annu Rev Genet. 2012; 46:515–536. [PubMed: 22974303]

Caimano MJ, Dunham-Ems S, Allard AM, Cassera MB, Kenedy M, Radolf JD. Cyclic di-GMP modulates gene expression in Lyme disease spirochetes at the tick-mammal interface to promote spirochete survival during the blood meal and tick-to-mammal transmission. Infect Immun. 2015; 83:3043–3060. [PubMed: 25987708]

Chaban B, Hughes HV, Beeby M. The flagellum in bacterial pathogens: for motility and a whole lot more. Semin Cell Dev Biol. 2015; 46:91–103. [PubMed: 26541483]

Charon NW, Cockburn A, Li C, Liu J, Miller KA, Miller MR, et al. The unique paradigm of spirochete motility and chemotaxis. Annu Rev Microbiol. 2012; 66:349–370. [PubMed: 22994496]

Charon NW, Goldstein SF, Marko M, Hsieh C, Gebhardt LL, Motaleb MA, et al. The flat-ribbon configuration of the periplasmic flagella of *Borrelia burgdorferi* and its relationship to motility and morphology. J Bacteriol. 2009; 191:600–607. [PubMed: 19011030]

Chen S, Beeby M, Murphy GE, Leadbetter JR, Hendrixson DR, Briegel A, et al. Structural diversity of bacterial flagellar motors. EMBO J. 2011; 30:2972–2981. [PubMed: 21673657]

Chevance FF, Hughes KT. Coordinating assembly of a bacterial macromolecular machine. Nat Rev Microbiol. 2008; 6:455–465. [PubMed: 18483484]

Dresser AR, Hardy P, Chaconas G. Investigation of the genes involved in antigenic switching at the *vlsE* locus in *Borrelia burgdorferi*: an essential role for the RuvAB branch migrase. PLoS Pathog. 2009; 5:e1000680. [PubMed: 19997508]

Elias AF, Bono JL, Kupko JJ 3rd, Stewart PE, Krum JG, Rosa PA. New antibiotic resistance cassettes suitable for genetic studies in *Borrelia burgdorferi*. J Mol Microbiol Biotechnol. 2003; 6:29–40. [PubMed: 14593251]

Elias AF, Stewart PE, Grimm D, Caimano MJ, Eggers CH, Tilly K, et al. Clonal polymorphism of *Borrelia burgdorferi* strain B31 MI: implications for mutagenesis in an infectious strain background. Infect Immun. 2002; 70:2139–2150. [PubMed: 11895980]

Fraser CM, Casjens S, Huang WM, Sutton GG, Clayton R, Lathigra R, et al. Genomic sequence of a Lyme disease spirochaete, *Borrelia burgdorferi*. Nature. 1997; 390:580–586. [PubMed: 9403685]

Fukuoka H, Wada T, Kojima S, Ishijima A, Homma M. Sodium-dependent dynamic assembly of membrane complexes in sodium-driven flagellar motors. Mol Microbiol. 2009; 71:825–835. [PubMed: 19183284]

Ge Y, Charon NW. Identification of a large motility operon in *Borrelia burgdorferi* by semi-random PCR chromosome walking. Gene. 1997; 189:195–201. [PubMed: 9168127]

Ge Y, Old IG, Saint Girons I, Charon NW. Molecular characterization of a large *Borrelia burgdorferi* motility operon which is initiated by a consensus sigma70 promoter. J Bacteriol. 1997; 179:2289–2299. [PubMed: 9079915]

Hu B, Morado DR, Margolin W, Rohde JR, Arizmendi O, Picking WL, et al. Visualization of the type III secretion sorting platform of *Shigella flexneri*. Proc Natl Acad Sci U S A. 2015; 112:1047–1052. [PubMed: 25583506]

Hyde JA, Shaw DK, Smith R III, Trzeciakowski JP, Skare JT. The BosR regulatory protein of *Borrelia burgdorferi* interfaces with the RpoS regulatory pathway and modulates both the oxidative stress response and pathogenic properties of the Lyme disease spirochete. Mol Microbiol. 2009; 74:1344–1355. [PubMed: 19906179]

Iyer R, Caimano MJ, Luthra A, Axline D, Corona A, Iacobas DA, et al. Stage-specific global alterations in the transcriptomes of Lyme disease spirochetes during tick feeding and following mammalian host adaptation. Mol Microbiol. 2015; 95:509–538. [PubMed: 25425211]

Jenal U, White J, Shapiro L. *Caulobacter* flagellar function, but not assembly, requires FliL, a non-polarly localized membrane protein present in all cell types. J Mol Biol. 1994; 243:227–244. [PubMed: 7932752]

Kojima S. Dynamism and regulation of the stator, the energy conversion complex of the bacterial flagellar motor. Curr Opin Microbiol. 2015; 28:66–71. [PubMed: 26457925]

Kojima S, Blair DF. Solubilization and purification of the MotA/MotB complex of *Escherichia coli*. Biochemistry (N Y). 2004; 43:26–34.

Kremer JR, Mastronarde DN, McIntosh JR. Computer visualization of three-dimensional image data using IMOD. J Struct Biol. 1996; 116:71–76. [PubMed: 8742726]

Krogh A, Larsson B, Von Heijne G, Sonnhammer EL. Predicting transmembrane protein topology with a hidden Markov model: application to complete genomes. J Mol Biol. 2001; 305:567–580. [PubMed: 11152613]

Kudryashev M, Cyrklaff M, Baumeister W, Simon MM, Wallich R, Frischknecht F. Comparative cryo-electron tomography of pathogenic Lyme disease spirochetes. Mol Microbiol. 2009; 71:1415–1434. [PubMed: 19210619]

Kudryashev M, Cyrklaff M, Wallich R, Baumeister W, Frischknecht F. Distinct in situ structures of the *Borrelia* flagellar motor. J Struct Biol. 2010; 169:54–61. [PubMed: 19699799]

Kuehn BM. CDC estimates 300,000 US cases of Lyme disease annually. JAMA. 2013; 310:1110. [PubMed: 24045727]

Leake MC, Chandler JH, Wadhams GH, Bai F, Berry RM, Armitage JP. Stoichiometry and turnover in single, functioning membrane protein complexes. Nature. 2006; 443:355–358. [PubMed: 16971952]

Li C, Bakker RG, Motaleb MA, Sartakova ML, Cabello FC, Charon NW. Asymmetrical flagellar rotation in *Borrelia burgdorferi* nonchemotactic mutants. Proc Natl Acad Sci U S A. 2002; 99:6169–6174. [PubMed: 11983908]

Liu J, Howell JK, Bradley SD, Zheng Y, Zhou ZH, Norris SJ. Cellular architecture of *Treponema pallidum*: novel flagellum, periplasmic cone, and cell envelope as revealed by cryo electron tomography. J Mol Biol. 2010; 403:546–561. [PubMed: 20850455]

Liu J, Lin T, Botkin DJ, McCrum E, Winkler H, Norris SJ. Intact flagellar motor of *Borrelia burgdorferi* revealed by cryo-electron tomography: evidence for stator ring curvature and rotor/C-ring assembly flexion. J Bacteriol. 2009; 191:5026–5036. [PubMed: 19429612]

Mead PS. Epidemiology of Lyme Disease. Infect Dis Clin North Am. 2015; 29:187–210. [PubMed: 25999219]

Miller CL, Karna S, Seshu J. *Borrelia* host adaptation Regulator (BadR) regulates *rpoS* to modulate host adaptation and virulence factors in *Borrelia burgdorferi*. Mol Microbiol. 2013; 88:105–124. [PubMed: 23387366]

Minamino T, Imada K. The bacterial flagellar motor and its structural diversity. Trends Microbiol. 2015; 23:267–274. [PubMed: 25613993]

Moon K, Hobbs G, Motaleb MA. *Borrelia burgdorferi* CheD promotes various functions in chemotaxis and pathogenic life cycle of the spirochete. Infec Immun. 2016; 84:1743–1752. [PubMed: 27021244]

Motaleb MA, Miller MR, Bakker RG, Li C, Charon NW. Isolation and Characterization of Chemotaxis Mutants of the Lyme Disease Spirochete *Borrelia burgdorferi* Using Allelic Exchange Mutagenesis, Flow Cytometry, and Cell Tracking. Meth Enzymol. 2007; 422:419–437.

Motaleb MA, Corum L, Bono JL, Elias AF, Rosa P, Samuels DS, Charon NW. *Borrelia burgdorferi* periplasmic flagella have both skeletal and motility functions. Proc Natl Acad Sci U S A. 2000; 97:10899–10904. [PubMed: 10995478]

Motaleb MA, Pitzer JE, Sultan SZ, Liu J. A novel gene inactivation system reveals altered periplasmic flagellar orientation in a *Borrelia burgdorferi fliL* mutant. J Bacteriol. 2011; 193:3324–3331. [PubMed: 21441522]

Motaleb M, Liu J, Wooten RM. Spirochetal motility and chemotaxis in the natural enzootic cycle and development of Lyme disease. Curr Opin Microbiol. 2015; 28:106–113. [PubMed: 26519910]

Murphy GE, Leadbetter JR, Jensen GJ. *In situ* structure of the complete *Treponema primitia* flagellar motor. Nature. 2006; 442:1062–1064. [PubMed: 16885937]

Pappas CJ, Iyer R, Petzke MM, Caimano MJ, Radolf JD, Schwartz I. *Borrelia burgdorferi* requires glycerol for maximum fitness during the tick phase of the enzootic cycle. PLoS Pathog. 2011; 7:e1002102. [PubMed: 21750672]

Partridge JD, Nieto V, Harshey RM. A new player at the flagellar motor: FliL controls both motor output and bias. MBio. 2015; 6:e02367–14. [PubMed: 25714720]

Paulick A, Koerdt A, Lassak J, Huntley S, Wilms I, Narberhaus F, Thormann KM. Two different stator systems drive a single polar flagellum in *Shewanella oneidensis* MR-1. Mol Microbiol. 2009; 71:836–850. [PubMed: 19170881]

Pettersen EF, Goddard TD, Huang CC, Couch GS, Greenblatt DM, Meng EC, Ferrin TE. UCSF Chimera—a visualization system for exploratory research and analysis. J Comput Chem. 2004; 25:1605–1612. [PubMed: 15264254]

Pitzer JE, Sultan SZ, Hayakawa Y, Hobbs G, Miller MR, Motaleb MA. Analysis of the *Borrelia burgdorferi* cyclic-di-GMP-binding protein PlzA reveals a role in motility and virulence. Infect Immun. 2011; 79:1815–1825. [PubMed: 21357718]

Raddi G, Morado DR, Yan J, Haake DA, Yang XF, Liu J. Three-dimensional structures of pathogenic and saprophytic *Leptospira* species revealed by cryo-electron tomography. J Bacteriol. 2012; 194:1299–1306. [PubMed: 22228733]

Rogers EA, Terekhova D, Zhang H, Hovis KM, Schwartz I, Marconi RT. Rrp1, a cyclic-di-GMP-producing response regulator, is an important regulator of *Borrelia burgdorferi* core cellular functions. Mol Microbiol. 2009; 71:1551–1573. [PubMed: 19210621]

Sonnhammer EL, Von Heijne G, Krogh A. A hidden Markov model for predicting transmembrane helices in protein sequences. Proc Int Conf Intell Syst Mol Biol. 1998; 6:175–182. [PubMed: 9783223]

Sowa Y, Berry RM. Bacterial flagellar motor. Q Rev Biophys. 2008; 41:103–132. [PubMed: 18812014]

Stewart PE, Bestor A, Cullen JN, Rosa PA. A tightly regulated surface protein of *Borrelia burgdorferi* is not essential to the mouse-tick infectious cycle. Infect Immun. 2008; 76:1970–1978. [PubMed: 18332210]

Suaste-Olmos F, Domenzain C, Mireles-Rodriguez JC, Poggio S, Osorio A, Dreyfus G, Camarena L. The flagellar protein FliL is essential for swimming in *Rhodobacter sphaeroides*. J Bacteriol. 2010; 192:6230–6239. [PubMed: 20889747]

Sultan SZ, Pitzer JE, Miller MR, Motaleb MA. Analysis of a *Borrelia burgdorferi* phosphodiesterase demonstrates a role for cyclic-di-guanosine monophosphate in motility and virulence. Mol Microbiol. 2010; 77:128–142. [PubMed: 20444101]

Sultan SZ, Manne A, Stewart PE, Bestor A, Rosa PA, Charon NW, Motaleb MA. Motility is crucial for the infectious life cycle of *Borrelia burgdorferi*. Infect Immun. 2013; 81:2012–2021. [PubMed: 23529620]

Sultan SZ, Pitzer JE, Boquoi T, Hobbs G, Miller MR, Motaleb MA. Analysis of the HD-GYP domain cyclic dimeric GMP phosphodiesterase reveals a role in motility and the enzootic life cycle of *Borrelia burgdorferi*. Infect Immun. 2011; 79:3273–3283. [PubMed: 21670168]

Sultan SZ, Sekar P, Zhao X, Manne A, Liu J, Wooten RM, Motaleb MA. Motor rotation is essential for the formation of the periplasmic flagellar ribbon, cellular morphology, and *Borrelia burgdorferi* persistence within *Ixodes scapularis* tick and murine hosts. Infect Immun. 2015; 83:1765–1777. [PubMed: 25690096]

Wolgemuth CW. Flagellar motility of the pathogenic spirochetes. Semin Cell Dev Biol. 2015; 46:104–112. [PubMed: 26481969]

Zhang X, Meltzer MI, Pena CA, Hopkins AB, Wroth L, Fix AD. Economic impact of Lyme disease. Emerg Infect Dis. 2006; 12:653–660. [PubMed: 16704815]

Zhao X, Norris SJ, Liu J. Molecular architecture of the bacterial flagellar motor in cells. Biochemistry. 2014; 53:4323–4333. [PubMed: 24697492]

Zhao X, Zhang K, Boquoi T, Hu B, Motaleb MA, Miller KA, et al. Cryoelectron tomography reveals the sequential assembly of bacterial flagella in *Borrelia burgdorferi*. Proc Natl Acad Sci U S A. 2013; 110:14390–14395. [PubMed: 23940315]

Zhu S, Kumar A, Kojima S, Homma M. FliL associates with the stator to support torque generation of the sodium-driven polar flagellar motor of *Vibrio*. Mol Microbiol. 2015; 98:101–110. [PubMed: 26103585]

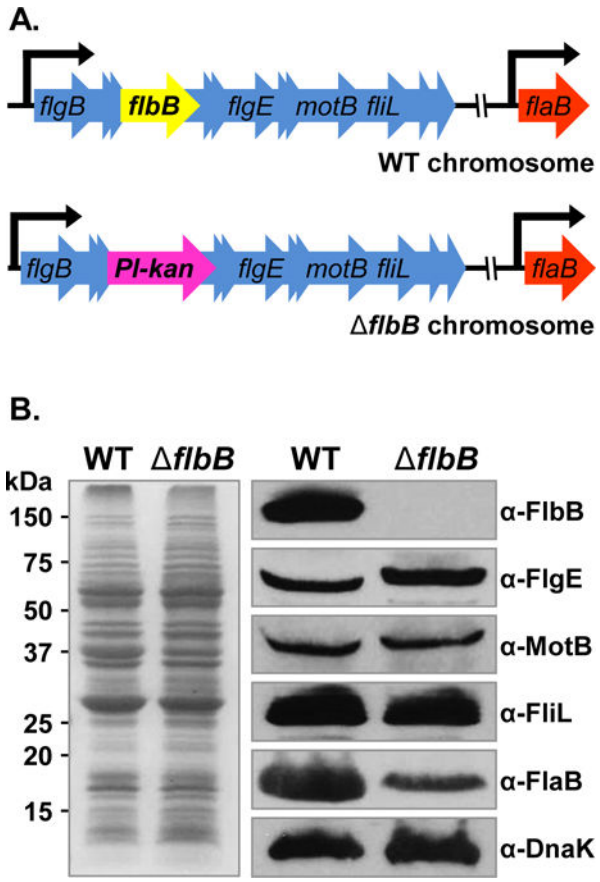

Figure 1. Construction of Δ*flbB* mutant and determination of polar effect on downstream genes expression

(A) Schematic diagrams of wild-type and Δ*flbB* mutant genomes. *flaB* gene (*bb0147*) is separated from the targeted *flbB* gene (*bb0286*) by approximately 100 kb. WT *B. burgdorferi* with the *flgB* polycistronic operon containing the targeted *flbB* is shown in top panel. The *Pl-kan* cassette replacing the *flbB* gene by allelic exchange is shown in bottom panel. The model lists only a few of the 26 genes of the *flgB* operon, and other genes are indicated by multiple arrowheads. (B) Confirmation of *flbB* gene-deletion and determination of polar effect by western blotting. WT and Δ*flbB* mutant cell lysates were subjected to SDS-PAGE (left) followed by immunoblotting (right). Immunoblotting was performed with *B. burgdorferi* FlbB, FlgE, MotB, FliL, or FlaB-specific antibodies. DnaK was used as a loading control. FlbB antiserum reacted with a 14 kDa protein in the wild-type lysate that is absent in the Δ*flbB* lysates indicate that this protein is the FlbB (FlbB blot).

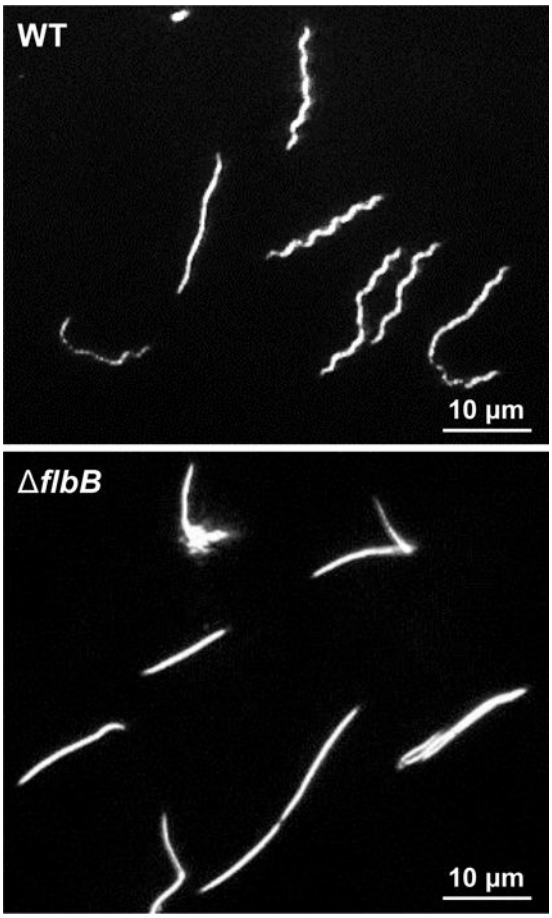

Figure 2. Morphology phenotype of the Δ*flbB* mutant cells

Dark-field microscopic images showing the distinct rod-shaped morphology of ΔflbB spirochetes whereas the wild-type (WT) cells exhibit a flat-wave morphology. Growing *B. burgdorferi* cells were visualized using a dark-field microscope (40×) and images were captured using a digital camera. The mutant cells were also non-motile (see Fig. S1).

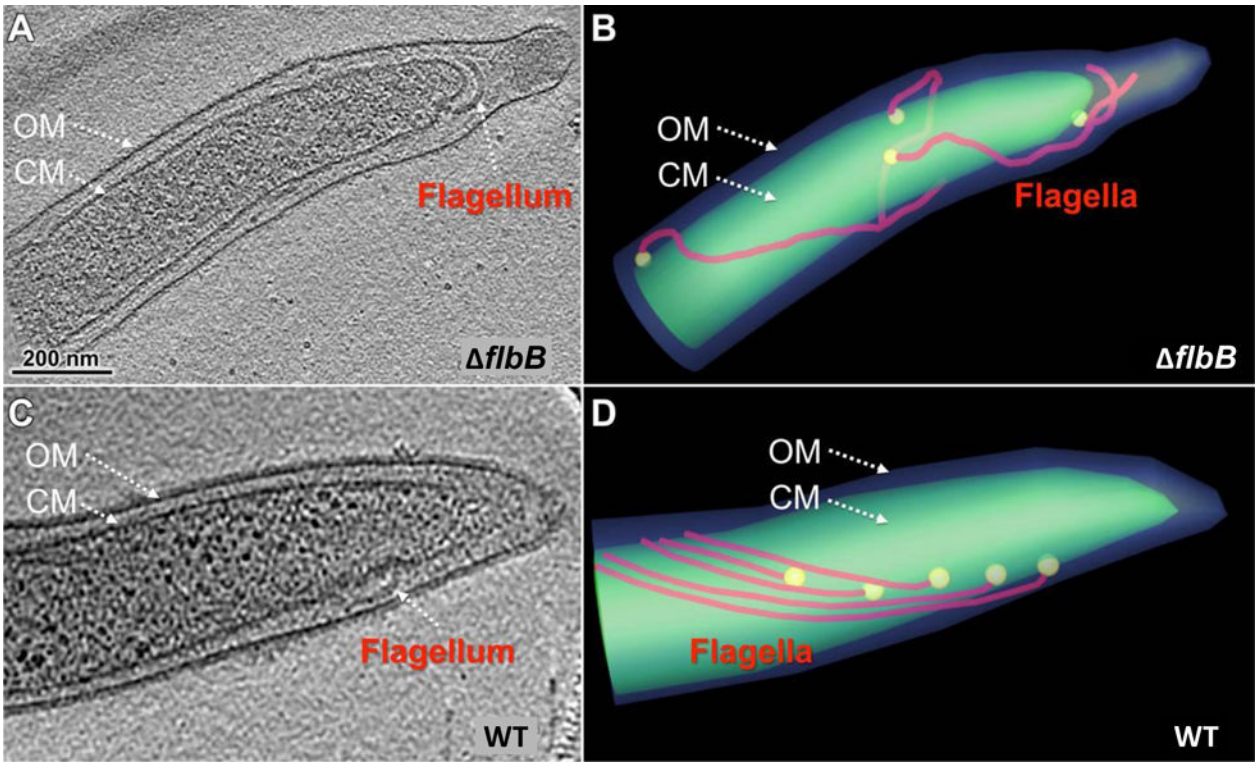

Figure 3. Periplasmic flagellar orientation in wild-type and Δ*flbB* mutant

(A) A representative tomographic slice of a Δ*flbB* cell showing that the periplasmic flagella are abnormally oriented toward the cell pole. (B) A cartoon model of the Δ*flbB* mutant shown in (A) clearly illustrated the abnormal tilting of the flagella. (C) A representative tomographic slice of a WT cell showing the periplasmic flagella that are extended toward the cell body but not the cell pole. (D) A cartoon model of the WT cell showing the normal orientation of the flagella toward the cell body.

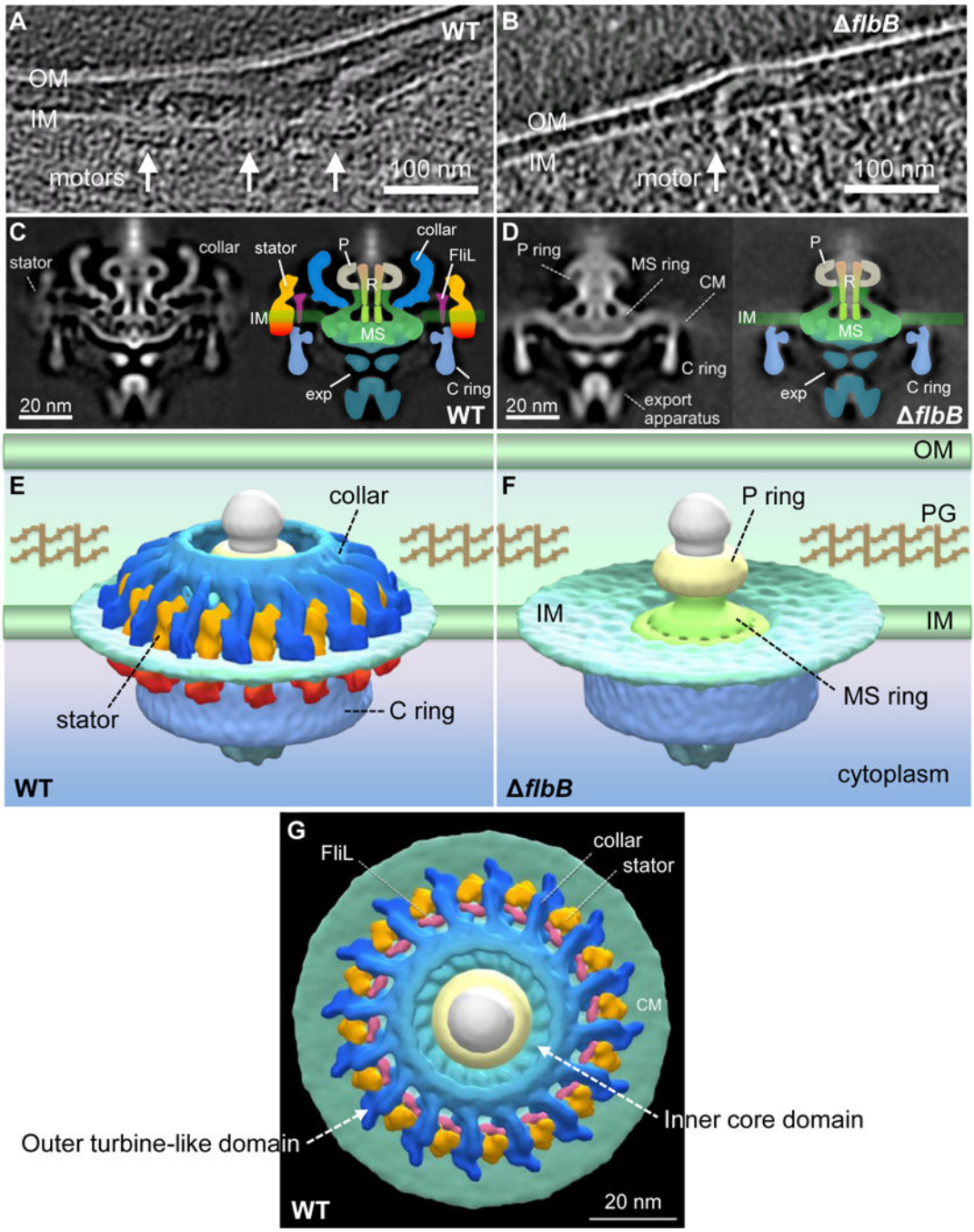

Figure 4. Comparative analysis of *in situ* flagellar motors from wild-type and Δ*flbB* reveals the 3D collar structure for the first time

(A) A tomographic section from a WT cell shows the motors that are embedded in the cytoplasmic inner membrane (IM/CM). (B) A tomographic section from a Δ*flbB* cell shows a motor that is embedded in the cytoplasmic membrane. (C) The central section (left) and schematic diagram (right) of the WT flagellar motor. (D) The central section (left) and schematic diagram (right) of the Δ*flbB* flagellar motor. (E) The surface rendering of the 3D averaged WT and (F) Δ*flbB* motor structures are shown in side view. (G) The surface rendering of the 3D averaged WT motor structure is shown in tilted top view (90°).

Compared to the motor structures from WT (C, E, G), the Δ*flbB* motor lacks the entire collar (blue), the stator (orange-red), and FliL (pink) structures. Noticeably, the collar is a large and complex structure comparing to FliL and the stator. OM, outer membrane; PG, peptidoglycan; P, P-ring; R, central rod; exp, export apparatus.

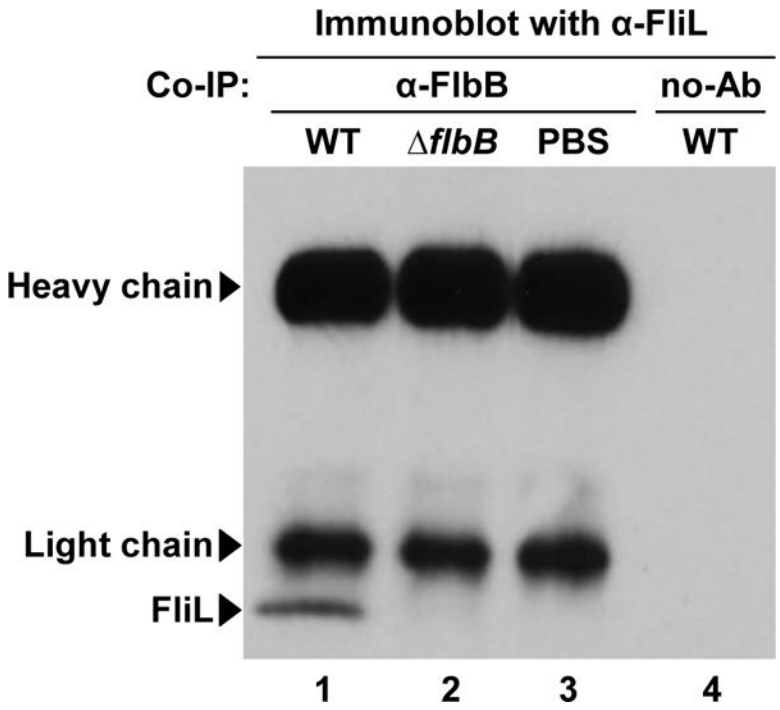

Figure 5. FlbB directly interacts with FliL

A co-IP assay showing the interaction between FlbB and FliL. FlbB-specific antibody conjugated with Dynabeads was incubated with wild-type or Δ*flbB* cell extracts. The proteins that were immunoprecipitated with the FlbB-antibody were separated using a gel, transferred to a PVDF-membrane, and subsequently, the membrane was blotted with anti-FliL (Motaleb *et al.*, 2011). FliL proteins are co-precipitated with *B. burgdorferi* wild-type cell extracts (lane 1), but not with Δ*flbB* mutant extracts (lane 2). PBS buffer was used as a negative control (lane 3). To check for the non-specific protein binding on Dynabeads, we used empty Dynabeads (no Ab/antisera) in the co-IP with wild-type extracts (lane 4). Arrowheads indicate the positions of antibody heavy chain (~55 kDa), light chain (~25 kDa), or FliL (~20 kDa). Lane numbers are shown at the bottom of the figure. See also Figure S2.

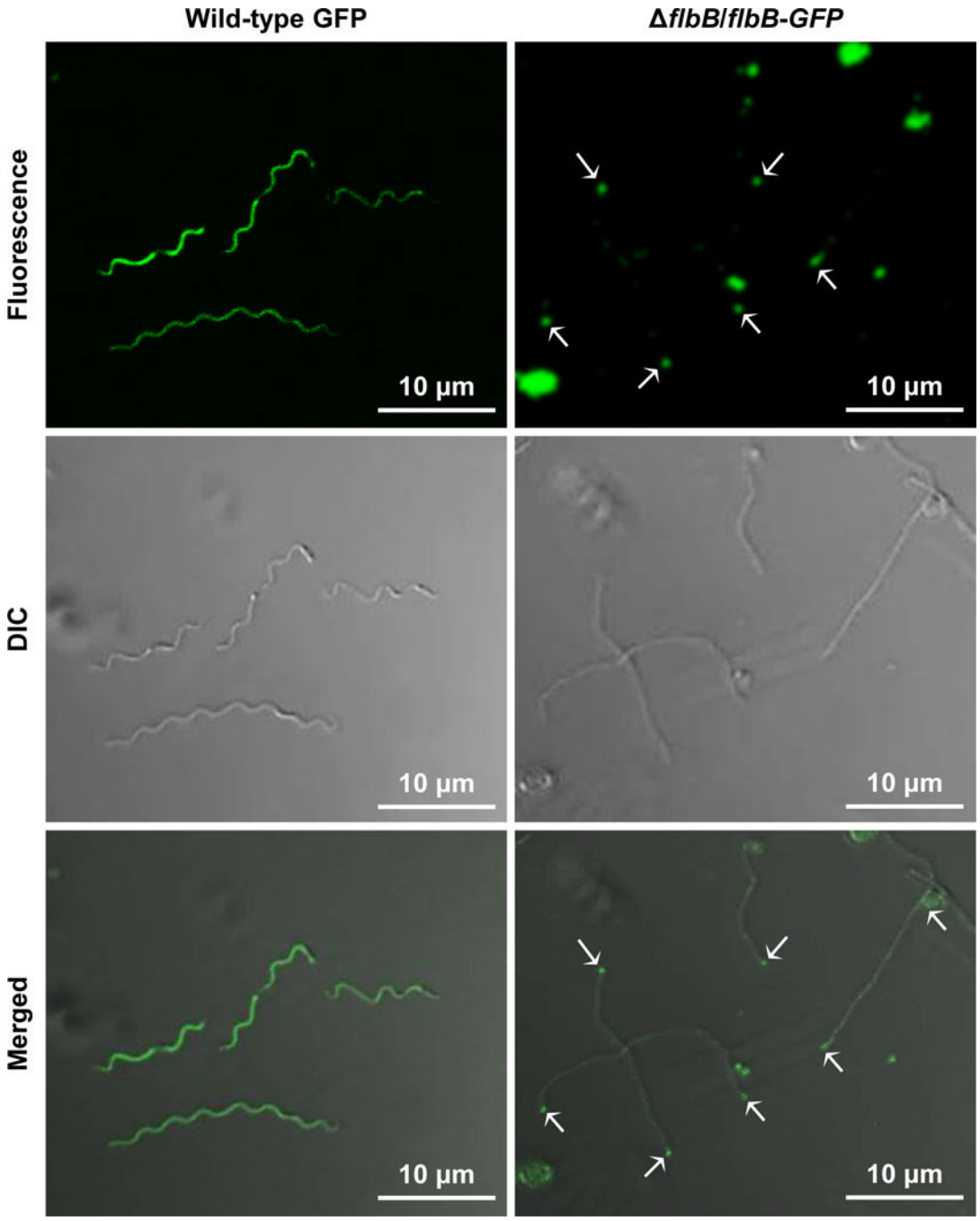

Figure 6. Expression and location of FlbB-GFP in *B. burgdorferi*

Confocal microscopy showing the fluorescence (top), differential interference contrast (DIC; middle), and merged (bottom) micrographs of the wild-type cells expressing GFP (wild-type GFP) and of Δ*flbB* cells expressing FlbB-GFP (Δ*flbB/flbB-GFP*) at 64×. The white arrows indicate the location of FlbB-GFP in the Δ*flbB/flbB-GFP* cell tips (FlbB-GFP clusters were detected in approximately 73% cells tips). Even distribution of the GFP signal was observed throughout the wild-type GFP cells, as expected.

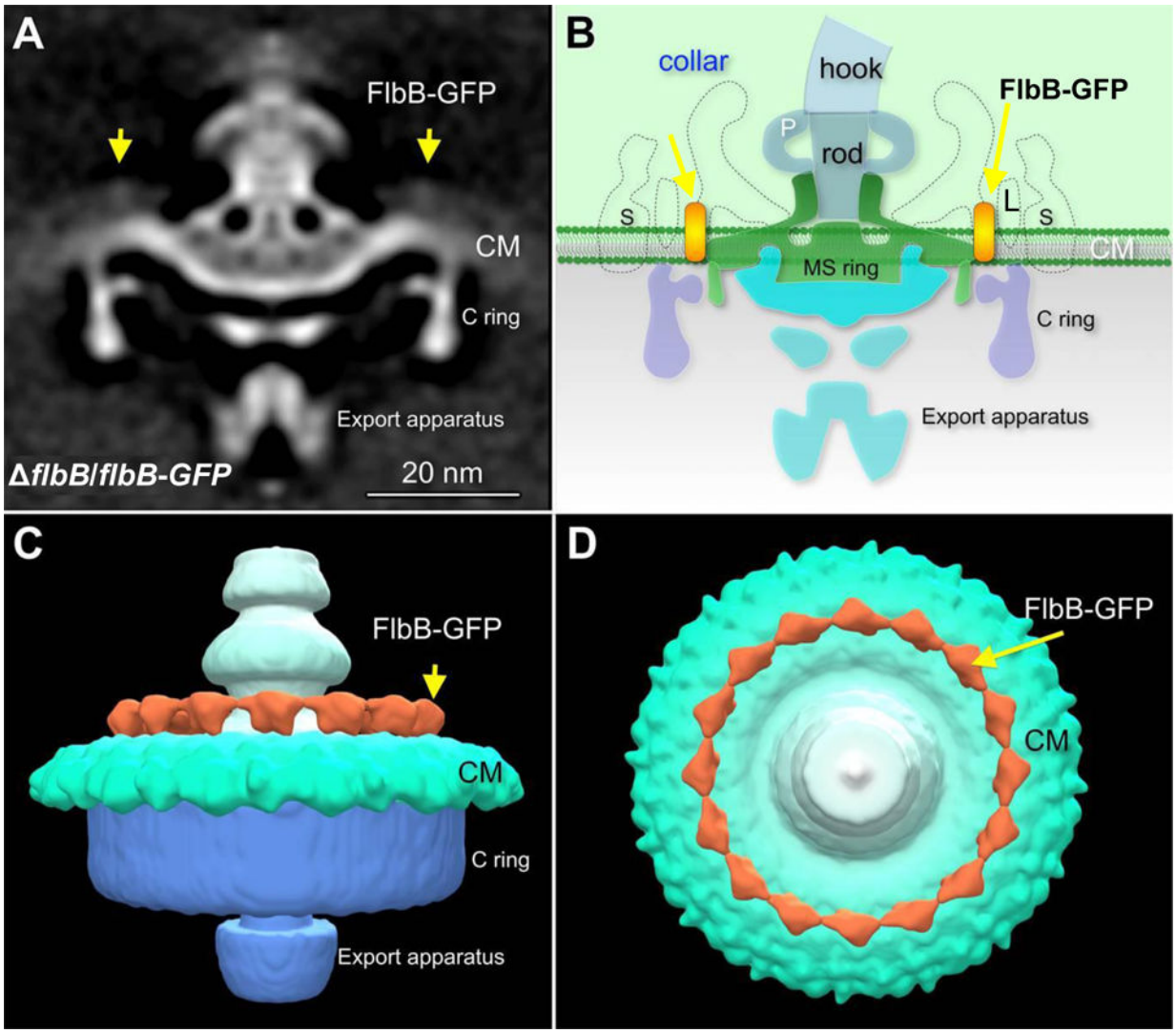

Figure 7. Location of FlbB-GFP as determined by cryo-ET

(A) The averaged 3D motor structures of the Δ*flbB* cells expressing FlbB-GFP (Δ*flbB/flbB-GFP*), and (B) schematic diagram of the Δ*flbB/flbB-GFP* flagellar motor illustrating the location of FlbB at the base of the collar. (C) Three dimensional isosurface rendering of the Δ*flbB/flbB-GFP* flagellar motor is shown in side view. (D) Three dimensional isosurface rendering of the Δ*flbB/flbB-GFP* flagellar motor is shown in tilted (top) view. The yellow arrows indicate the location of FlbB-GFP. S, stator; L, FliL; P, P-ring.

Table 1

Periplasmic flagella of Δ*flbB* mutant cells are oriented abnormally toward the cell pole.

Strain	No. of cells analyzed	No. of irregular periplasmic flagella[a]	No. of normal periplasmic flagella[b]	% irregular periplasmic flagella
Wild-type	43	5	288	1.7
Δ*fliL*	41	55	208	21
Δ*flbB*	44	144	32	82

[a] Irregular periplasmic flagella were tilted toward the cell pole.

[b] Normal periplasmic flagella were tilted toward the cell body. Δ*fliL* mutant was used as a reference strain (Motaleb *et al.*, 2011).